

Autoencoder-based background reconstruction and foreground segmentation with background noise estimation

Bruno Sauvalle and Arnaud de La Fortelle

Mines ParisTech PSL University 75006 Paris France

`bruno.sauvalle@mines-paristech.fr`

Abstract. Even after decades of research, dynamic scene background reconstruction and foreground object segmentation are still considered as open problems due various challenges such as illumination changes, camera movements, or background noise caused by air turbulence or moving trees. We propose in this paper to model the background of a frame sequence as a low dimensional manifold using an autoencoder and compare the reconstructed background provided by this autoencoder with the original image to compute the foreground/background segmentation masks. The main novelty of the proposed model is that the autoencoder is also trained to predict the background noise, which allows to compute for each frame a pixel-dependent threshold to perform the foreground segmentation. Although the proposed model does not use any temporal or motion information, it exceeds the state of the art for unsupervised background subtraction on the CDnet 2014 and LASIESTA datasets, with a significant improvement on videos where the camera is moving. It is also able to perform background reconstruction on some non-video image datasets.

Keywords: background reconstruction, background subtraction, unsupervised object detection, video surveillance

1 Introduction

We consider in this paper the tasks of dynamic background reconstruction and foreground/background segmentation. The dynamic background reconstruction task can be described in the following way: The input is a sequence \mathcal{X} of consecutive frames X_1, \dots, X_N showing a scene cluttered by various moving objects, such as cars or pedestrians, and the expected output is a sequence $\hat{\mathcal{X}} = \hat{X}_1, \dots, \hat{X}_N$ of frames showing the backgrounds of each scene without those objects. If the camera is fixed and the illumination conditions do not change, the various frames $\hat{X}_1, \dots, \hat{X}_N$ will be nearly identical. However if this is not the case, then these frames can be very different from each other. The foreground/background segmentation task similarly takes as input the same kind of frames sequence X_1, \dots, X_N , but the expected output is a sequence \mathcal{M} of foreground masks M_1, \dots, M_N whose values at the pixel p are equal to zero if this pixel

shows the background in the considered frame, and equal to 1 if the background is masked by a foreground moving object at this pixel (Fig. 1).

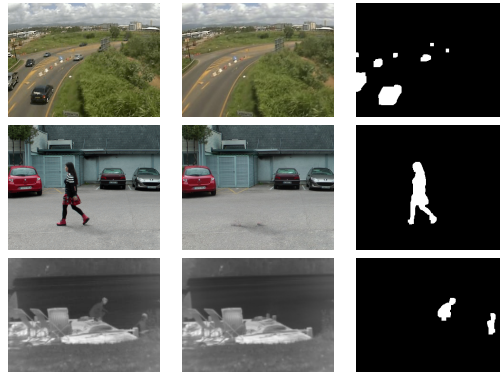


Fig. 1. The proposed model takes as input a frame from the associated video (left column) and provides a reconstruction of the background (middle column) and a foreground mask (right column).

This task is often called background subtraction because the pointwise multiplication of the mask M_k and the input image X_k gives an image showing only the foreground moving objects present in X_k , the input image background being replaced by a black background. The applications of background subtraction are very diverse [19]: road, airport, store, maritime or military surveillance, observation of animals and insects, motion capture, human-computer interface, video matting, fire detection... Although the task of automatic background subtraction has been studied for more than 30 years [63], it is still considered as an open problem due to the various challenges appearing in real applications: illumination changes, high level of occlusion of the background, background motions caused by moving trees or water, challenging weather conditions, presence of shadows... Dynamic background reconstruction models have been used for background subtraction, but are now also implemented as components of unsupervised object detection and tracking models [27,23,65].

The model presented in this paper starts from the classical assumption that the dynamic background of a scene can be modeled as a low dimensional manifold and uses an autoencoder to learn this manifold and perform dynamic background reconstruction. It then compares the input frame with the associated background predicted by the autoencoder to build the foreground/segmentation mask. The main contributions of this paper are the following :

- We implement a new loss function to train the autoencoder, which gives a high weight to reconstruction errors associated to background pixels and a low weight to reconstruction errors associated to foreground pixels, and shows better performance than the L_1 loss usually considered for this task.

- We train the autoencoder to provide a background reconstruction, but also a background noise estimation, which gives a pixelwise estimate of the uncertainty of the background prediction. This noise estimation map is used to adjust the threshold necessary to compute the background/foreground segmentation mask.
- We reduce the risk of overfitting by implementing an early stopping criterion and adapting the autoencoder parameter count to the complexity of the background sequence.

The paper is structured as follows : We first review related work in section 2, then describe the proposed model in section 3. Experimental results on various datasets are then provided in section 4.

2 Related work

Background subtraction methods can be split between supervised methods, which require labeled data, and unsupervised methods. Fully unsupervised methods are methods which do not require training data and can be applied to any video sequence without any update of the model parameters.

One can classify unsupervised methods as statistical methods or reconstruction methods. Statistical methods rely on a statistical modeling of the distribution of background pixel color values or other local features to predict whether a particular pixel is foreground or background. These statistical models can be parametric (univariate gaussian [63], mixture of gaussians [56], clusters [36], Student’s t-distributions [44], Dirichlet process mixture models [5], Poisson mixture models [18], asymmetric generalized gaussian mixture models [15], etc.) or non parametric (pixel value histograms [68], kernel density estimation [14], codebooks [31], history of recently observed pixels [2,24], etc.). The efficiency of these methods can be increased by using as input not only the pixel color values, but also features attached to superpixels [11] or local descriptors which are robust to illumination changes, such as SIFT [52], LBP or LBSP descriptors. [54,55]. If the camera is static, the segmentation of moving objects on a scene can also be performed by evaluating the motion associated to each pixel, using optical flow or flux tensor models. The blobs produced by these models are generally very fuzzy, but can be used as input to more complex models [8,61]. Several unsupervised models can be also combined to form a more accurate ensemble model [4].

Reconstruction methods use a background reconstruction model to predict the color (or other features) of the background at a particular pixel. The difference between the current image and the predicted background is then computed and followed by a thresholding to decide whether the a pixel is background or foreground. Pixelwise reconstruction models try to predict the value of a background pixel at a particular frame using the sequence of values of the pixel of the last frames using a filter, which can be a Wiener filter [59], a Kalman filter [49] or a Chebychev filter [10]. A global prediction of the background can also be

performed using the assumption that the background frames form a low dimensional manifold, which motivates the use of dimensionality reduction techniques such as principal component analysis (PCA) [45]. One can add to this approach a prior on the sparsity of the foreground objects by using a L_1 loss term applied to the foreground residuals, which leads to the development of models based on robust principal component analysis (RPCA) [64,9]. More complex norms and additional regularizers have been proposed to improve the performance of this approach [40,37,66,26,25]. Non-linear dimensionality reduction using an autoencoder for background reconstruction has already been implemented [17,48] and is further developed in the proposed model.

Supervised methods require labeled data as input. The labeled data are sets of pairs (X_k, M_k) , where the image X_k is an image extracted from the sequence X_1, \dots, X_N and the foreground mask M_k has to be provided by a human intervention. Supervised algorithms using linear methods such as as maximum margin criterion [33,13] or graph signal reconstruction methods [20] have been proposed, but the current best performing supervised models use deep learning techniques with convolutional encoder-decoder structures [35,34,41], U-net structures [47,43] or GANs [57,69].

Although supervised models can reach very high accuracy results on a given video after training, their ability to generalize to new videos remain a major issue, and evaluation on unseen scenes may lead to unfavorable results compared to unsupervised algorithms [41]. A spatio-temporal data augmentation strategy has been proposed [58] to improve generalization. One can also use as additional input to the deep learning model the output of an unsupervised background subtraction model [47,46]. A background subtraction model can also be substantially improved by combining its results with the output of a supervised semantic segmentation model [7,67].

Several surveys [6,43,29,42] discuss background reconstruction and background subtraction models.

3 Model description

The proposed model is a reconstruction model and has a general structure similar to the DeepPBM model [17]: We assume that the background frames form a low dimensional manifold and train an autoencoder to learn this manifold from the complete video using a reconstruction loss. We however observe that the DeepPBM model shows the following shortcomings:

- The structure of the autoencoder and the number of latent variables have to be defined on a scene by scene basis, which requires a human supervision. If the number of latent variables is too high, the autoencoder quickly learns to reproduce the foreground objects, a phenomenon we call overfitting, and fails to generate a proper background.
- This model is able to handle changes in lightning conditions, but struggles to handle camera movements.

- The thresholding mechanism is not able to cope with dynamic backgrounds such as clouds or trees, which leads to false detections.

In order to handle these issues, we implement the following features:

3.1 Reconstruction loss using background bootstrapping

We implement a reconstruction loss using background bootstrapping [50], which we found to be more efficient than the L_1 loss for dynamic background reconstruction. In the case of dynamic background reconstruction, this loss function allows to reduce the risk of overfitting to the foreground objects by giving a higher weight to background pixels than to foreground pixels during the optimization process.

The proposed reconstruction loss can be described by the following formulae:

We note $x_{n,c,i,j}$ the pixel color value of the image X_n for the channel c at the position (i, j) with $1 \leq c \leq 3, 1 \leq i \leq h$ and $1 \leq j \leq w$, and $\hat{x}_{n,c,i,j}$ the pixel value of the reconstructed background \hat{X}_n for the same color and position. The local l_1 error associated to the pixel (i, j) is

$$l_{n,i,j} = \sum_{c=1}^3 |\hat{x}_{n,c,i,j} - x_{n,c,i,j}|. \quad (1)$$

If at least one of the color channels give a high error, then $l_{n,i,j}$ is large and the pixel (i, j) of the image X_n is considered to be a foreground pixel. A soft foreground mask $m_n \in [0, 1]^{h \times w}$ for the image X_n is then computed using the formula

$$m_{n,i,j} = \tanh\left(\frac{l_{n,i,j}}{\tau_1}\right), \quad (2)$$

where τ_1 is some positive hyperparameter, which can be considered as a soft threshold. A spatially smoothed version $\tilde{m}_{n,i,j}$ of this mask is then computed by averaging using a square kernel of size $(2k+1) \times (2k+1)$, with $k = \lfloor w/r \rfloor$ (where w is the image width and r is some integer hyperparameter):

$$\tilde{m}_{n,i,j}(\hat{X}_n, X_n) = \frac{1}{(2k+1)^2} \sum_{l=-k, p=-k}^{l=k, p=k} m_{n,i+l, j+p} \quad (3)$$

The associated pixel-wise weight $w_{n,i,j}^{\text{bootstrap}}$ is then defined as

$$w_{n,i,j}^{\text{bootstrap}} = e^{-\beta \tilde{m}_{n,i,j}}, \quad (4)$$

where β is some positive hyperparameter. The reconstruction loss of the auto-encoder is then computed by weighting the pixelwise L_1 losses $l_{n,i,j}$ using these bootstrap weights:

$$\mathcal{L}_{\text{rec}}(\hat{\mathcal{X}}, \mathcal{X}) = \frac{1}{Nhw} \sum_{n=1, i=1, j=1}^{N, h, w} w_{n,i,j}^{\text{bootstrap}} l_{n,i,j} \quad (5)$$

We do not use any optical flow or motion estimation input in the proposed model because we want it to be able to handle situations where the camera is moving.

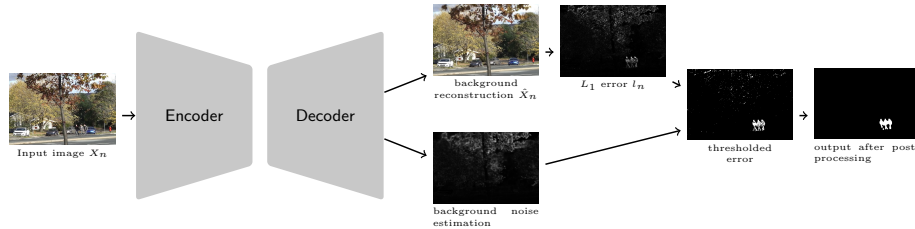


Fig. 2. Schematic of the proposed model during inference (Error and noise images are normalized in the range $[0,1]$)

3.2 Optimized thresholding using background noise estimation

We remark that the bootstrap pixel weights $w_{n,i,j}^{\text{bootstrap}}$ can be used to get an estimate of the level of background noise of a frame sequence, considering that these weights are close to one when the associated pixel is a background pixel, and close to zero when this is not the case.

We therefore add a fourth output channel to the auto-encoder, which is dedicated to give an estimate $\hat{l}_{n,i,j}$ of the value of the L_1 error $l_{n,i,j}$ for each pixel (i, j) for the frame X_n (Fig. 2).

The associated loss function is weighted using the bootstrap weights in order to limit its scope to background regions:

$$\mathcal{L}_{\text{noise}} = \frac{1}{3Nhw} \sum_{n=1}^{N,h,w} w_{n,i,j}^{\text{bootstrap}} |\hat{l}_{n,i,j} - l_{n,i,j}| \quad (6)$$

When the background is very noisy, the autoencoder is not able to predict accurately the value of a background pixel color. As a consequence, the expectation of $l_{n,i,j}$ is large, which leads to a high value of $\hat{l}_{n,i,j}$.

The autoencoder is trained using the sum of the reconstruction loss and the loss associated to the background noise estimation. The complete loss function is then

$$\mathcal{L} = \mathcal{L}_{\text{rec}} + \mathcal{L}_{\text{noise}}. \quad (7)$$

The gradients of the weights $w_{n,i,j}^{\text{bootstrap}}$ are not computed during the optimization process [50]. We also do not use the gradient of $l_{n,i,j}$ in equation 6 because we do not want the quality of the background reconstruction be impacted by the background noise estimation optimization process.

In order to set the pixelwise threshold $\tau_{n,i,j}$ associated to the pixel (i, j) of the frame X_n and necessary to compute the background/foreground segmentation mask, we also take into account the average illumination \hat{I}_n of the reconstructed background \hat{X}_n , as defined by the formula

$$\hat{I}_n = \frac{1}{3hw} \sum_{c=1, i=1, j=1}^{3, h, w} |\hat{x}_{n,c,i,j}|. \quad (8)$$

The threshold $\tau_{n,i,j}$ is then set according to the formula

$$\tau_{n,i,j} = \alpha_1 \hat{I}_n + \alpha_2 \hat{l}_{n,i,j}, \quad (9)$$

where α_1 and α_2 are two positive hyperparameters. The motivation of this formula is that if the background noise is very high at some pixel, we have to increase the associated threshold for background/foreground segmentation in order to prevent the misclassification of background pixels as foreground caused by background noise.

For a given frame sequence X_1, \dots, X_n and a reconstructed background sequence $\hat{X}_1, \dots, \hat{X}_n$, we then compute the foreground mask M_n before post-processing using the thresholding rule $M_{n,i,j} = 1$ if and only if $l_{n,i,j} > \tau_{n,i,j}$.

A post-processing is then applied in order to remove rain drops, snow flakes, and other spurious detections. It is composed of two morphological operations: a morphological closing using a 5×5 square structural element, followed by a morphological opening with a 7×7 square structural element.

3.3 Detecting complex background changes

The improved reconstruction loss function introduced in 3.1 reduces the risk of overfitting, but is not able to prevent it completely. We observe that the risk of overfitting increases when the number of optimization iterations and the number of parameters of the network increase. This is a significant issue because sequences showing background changes require a high number of training iterations and a model with a large number of parameters. In order to prevent overfitting, the number of training iterations and the complexity of the model are therefore adjusted to the complexity of the backgrounds sequence.

The main challenge here is to estimate without any human supervision whether the video shows substantial background changes or not. We observe however that the proposed model can be used to answer to this question. In order to do this, we first train the model for a fixed small number N_{eval} of iterations, which is however sufficient to get a rough evaluation of the background changes. Using this trained model, we compute B_{eval} reconstructed backgrounds \hat{X}_n using frames X_n sampled from the sequence \mathcal{X} . We then compute the temporal median \hat{X} of these backgrounds and compare this median background with the recon-

structed backgrounds \hat{X}_n , computing soft masks following the same method and parameters as in formula 1 and 2:

$$l_{n,i,j} = \sum_{c=1}^3 |\hat{x}_{c,i,j} - \hat{x}_{n,c,i,j}| \quad (10)$$

$$m_{n,i,j} = \tanh\left(\frac{l_{n,i,j}}{\tau_1}\right). \quad (11)$$

We then consider the average soft mask value over the B_{eval} reconstructed backgrounds

$$\bar{m} = \frac{1}{B_{\text{eval}}hw} \sum_{n,i,j}^{B_{\text{eval}},h,w} m_{n,i,j}. \quad (12)$$

If \bar{m} is higher than a threshold τ_0 , we consider that the background is a complex background. The partially trained model is discarded, a new autoencoder is created with more parameters and the number of training iterations is set to N_{complex} with a minimum of E_{complex} epochs for very long sequences.

If this ratio is lower than τ_0 , we consider that the background is a simple background, keep the partially trained model, and finish the training, with a total number of training iterations set to N_{simple} .

4 Experimental results

4.1 Evaluation method

We consider the following benchmark datasets for background subtraction: CD-NET 2014, LASIESTA and BMC 2012 and use the same model hyperparameters on these three datasets.

We use the public implementations of the algorithms PAWCS [55] and SuB-SENSE [54] provided with the BGS library [53] to get baseline performance estimates for these methods when they are not available. We rely on published results for the other state of the art methods which do not have public implementations.

We use the F-measure as main evaluation criteria. To compute the F-measure associated to a sequence of foreground masks predictions M_1, \dots, M_n , we first compute the sums TP, TN, FP, FN of the true positives, true negatives, false positives and false negatives associated to the sequence of masks M_1, \dots, M_n , and then compute the F-measure associated to this sequence as the harmonic mean of precision and recall, which can also be described by the formula

$$F = \frac{TP}{TP + \frac{1}{2}(FN + FP)}. \quad (13)$$

Implementation details and autoencoder architecture are described in the appendix.

4.2 CDnet 2014 dataset

The CDnet 2014 dataset ¹ [62] is composed of 53 videos, for a total of 153 278 frames, selected to cover the various challenges which have to be addressed for background subtraction: dynamic background (scenes with water or trees), camera jitter, intermittent object motion, presence of shadows, images captured by infrared cameras, challenging weather (snow, fog), images captured with a low frame rate, night images, images filmed by a pan-tilt-zoom camera, air turbulence. Ground truth foreground segmentation masks are provided for all frames of the dataset, with specific labels for shadow pixels which are not considered in the F-measure computation. We provide in Table 1 the F-measure results per category of the proposed model for each category of the CDnet 2014 dataset, with a comparison with the results obtained by other unsupervised models.

The proposed model, despite the various mechanisms implemented to limit overfitting, nevertheless suffers from overfitting when big foreground objects stay still or moves very slowly in a frame sequence. This phenomenon is observed on three sequences of the CDnet dataset, "office", "library" and "canoe" (3), although the associated backgrounds are correctly classified as simple by the model. As a consequence, the average F-score on corresponding categories "baseline", "thermal" and "dynamic backgrounds" are below the scores of other state of the art models.

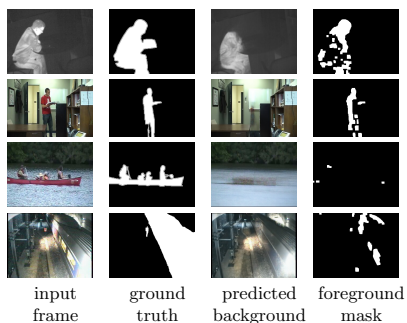


Fig. 3. Examples of overfitting on the datasets CDnet 2014 and BMC 2012 for the sequences "library", "office", "canoe" and "video007"

Despite this issue, the proposed model gets a higher average F-measure on the CDnet 2014 dataset than all published unsupervised models, with an average F-measure of 0.784. One can observe a significant improvement in accuracy with the proposed model in the "pan-tilt-zoom" (PTZ) category, showing that it is able to better handle situations where the camera is moving.

¹ <http://changedetection.net/>

Table 1. Comparison of top BGS algorithms according to the per-category F-measures on CDNet-2014 (sources : CDnet website <http://jacarini.dinf.usherbrooke.ca/results2014/1158/>, [26], [25]).

Method	Bad weatherline	Base-camera jitter	Camera motion backgr.	Dynamic obj. motion	Int. obj. framerate	Low	Night	PTZ	Shadow	Thermal	Turbulence	Overall
Unsupervised:												
AE-NE (ours)	0.8337	0.8959	0.9230	0.6225	0.8231	0.6771	0.5172	0.8000	0.8947	0.7999	0.8382	0.7841
IUTIS-5 [4]	0.8248	0.9567	0.8332	0.8902	0.7296	0.7743	0.5290	0.4282	0.9084	0.8303	0.7836	0.7717
WisenetMD [32]	0.8616	0.9487	0.8228	0.8376	0.7264	0.6404	0.5701	0.3367	0.8984	0.8152	0.8304	0.7535
SuBSENSE [54]	0.8619	0.9503	0.8152	0.8177	0.6569	0.6445	0.5599	0.3476	0.8986	0.8171	0.7792	0.7408
PAWCS [55]	0.8152	0.9397	0.8137	0.8938	0.7764	0.6588	0.4152	0.4615	0.8913	0.8324	0.6450	0.7403
C-EFIC [1]	0.7867	0.9309	0.8248	0.5627	0.6229	0.6806	0.6677	0.6207	0.8778	0.8349	0.6275	0.7307
MSCL [26]	0.83	0.87	0.83	0.85	0.80	n/a	n/a	n/a	0.82	0.80	0.80	n/a
B-SSSR [25]	0.92	0.97	0.93	0.95	0.74	n/a	n/a	n/a	0.93	0.86	0.87	n/a
Supervised:												
FgSegNet v2 [34]	0.9904	0.9978	0.9971	0.9951	0.9961	0.9336	0.9739	0.9862	0.9955	0.9938	0.9727	0.9847
BSUV-Net 2.0 [58]	0.8844	0.9620	0.9004	0.9057	0.8263	0.7902	0.5857	0.7037	0.9562	0.8932	0.8174	0.8387

4.3 LASIESTA dataset

The LASIESTA dataset² [12] is composed of 48 videos grouped in 14 categories, for a total of 18 425 video frames. All frames are provided with ground truth pixel labels, with a specific label for pixels associated to stopped moving objects which are excluded from the F-measure computation. We provide in Table 2 the average F-measure results of the proposed model for all 14 categories. Out of the 48 videos of the dataset, 4 videos are taken with a moving camera (categories IMC and OMC), and 24 videos include simulated camera motion (categories ISM and OSM). These 28 videos which include real or simulated camera motion are very difficult for existing background subtraction models and to our best knowledge, no paper has ever published category-wise evaluation results for these videos. In order to allow a comparison with these published results, we therefore also provide the average F-measure over the 10 categories showing only videos taken from a fixed camera. We observe that the proposed model performs slightly better than available unsupervised algorithms on static scenes, and with a significant improvement on scenes where the camera is moving.

4.4 BMC 2012 dataset

The BMC dataset³[60] contains 9 videos showing real scenes taken from static cameras and including the following challenges: shadows, snow, rain, presence of trees or big objects. Three of these sequences are very long (32 965, 117 149 and 107 815 frames). For fair comparison with other published results for this dataset, we provide the F-measure results for our model obtained using the usual F-measure definition described in 4.3, but also the results obtained using the executable evaluation tool provided with the dataset which does not use the same definition of the F-measure [60]. We compute SuBSENSE and PAWCS

² <https://www.gti.ssr.upm.es/data/>

³ <http://backgroundmodelschallenge.eu/>

Table 2. Average per category of video F-measures on LASIESTA (sources : [12],[3], authors experiments for PAWCS and SuBSENSE)

Method	static camera										moving camera or simulated motion				Average. 10 categ.	Average. 14 categ.
	ISI	ICA	IOC	IIL	IMB	IBS	OCL	ORA	OSN	OSU	IMC	ISM	OMC	OSM		
AE-NE (ours)	0.91	0.88	0.91	0.81	0.92	0.79	0.94	0.80	0.82	0.91	0.83	0.79	0.86	0.89	0.87	0.86
PAWCS [55]	0.90	0.88	0.90	0.79	0.81	0.79	0.96	0.93	0.69	0.82	0.48	0.77	0.43	0.75	0.85	0.78
SuBSENSE [54]	0.90	0.89	0.95	0.65	0.77	0.73	0.92	0.90	0.81	0.79	0.33	0.70	0.31	0.65	0.83	0.73
Cuevas [3]	0.88	0.84	0.78	0.65	0.93	0.66	0.93	0.87	0.78	0.72	n/a	n/a	n/a	n/a	0.81	n/a
Haines [22]	0.89	0.89	0.92	0.85	0.84	0.68	0.83	0.89	0.17	0.86	n/a	n/a	n/a	n/a	0.78	n/a
Maddalena [39]	0.95	0.86	0.95	0.21	0.91	0.40	0.97	0.90	0.81	0.88	n/a	n/a	n/a	n/a	0.78	n/a
Maddalena [38]	0.87	0.85	0.91	0.61	0.76	0.42	0.88	0.84	0.58	0.80	n/a	n/a	n/a	n/a	0.75	n/a

results on this dataset and provide published evaluation results for other models in 3.

Table 3. Comparison of top unsupervised BGS algorithms according to the video F-measure on BMC 2012

Method	Video 001	Video 002	Video 003	Video 004	Video 005	Video 006	Video 007	Video 008	Video 009	Average 9 videos
F-measure (as defined in equation 13)										
AE-NE (ours)	0.81	0.72	0.78	0.78	0.60	0.73	0.32	0.84	0.77	0.71
PAWCS [55]	0.70	0.58	0.85	0.72	0.27	0.79	0.58	0.74	0.80	0.67
SuBSENSE [54]	0.70	0.62	0.83	0.69	0.21	0.76	0.53	0.68	0.83	0.65
F-measure (using BMC evaluation tool)										
AE-NE (ours)	0.90	0.86	0.89	0.89	0.80	0.87	0.51	0.92	0.89	0.84
PAWCS [55]	0.86	0.77	0.93	0.86	0.66	0.89	0.79	0.87	0.90	0.84
SubSENSE [54]	0.85	0.80	0.92	0.85	0.68	0.87	0.75	0.84	0.91	0.83
DeepPBM [17]	0.73	0.86	0.94	0.90	0.71	0.81	0.70	0.76	0.69	0.78
G-LBM [48]	0.73	0.85	0.93	0.91	0.71	0.85	0.70	0.76	0.63	0.79
MSCL-FL [26]	0.84	0.84	0.88	0.90	0.83	0.80	0.78	0.85	0.94	0.86
B-SSSR [25]	n/a	0.88								

We remark that the F-measure associated to the proposed model is significantly below the state of the art on video 007. This video includes a sequence showing a train passing on the right lane and occupying a large part of the image (Table 3, last row). As noted earlier, the proposed model is prone to overfitting when large foreground objects appear to be static in a video, which is the case here due to the uniform texture of the train and leads to the train being integrated to the background. Despite this issue, the proposed model gets a competitive average F-measure on the dataset. It also improves upon the state of the art on videos 001 and 008.

4.5 Non-video image datasets : Clevrtex, ObjectsRoom, ShapeStacks

The proposed model, which does not use any temporal information, can be adapted to perform background reconstruction and foreground segmentation on some image datasets which are not extracted from video sequences. We have

tested this approach on three synthetic images datasets : Clevrtex⁴ [30], ShapeStacks⁵, [21] and ObjectsRoom⁶ [28]. We use on ShapeStacks and ObjectsRoom the same preprocessing as in [16]⁷. Although each image of these datasets shows a different background, the model is able to recognize that all the backgrounds appearing in a given dataset lie in a low dimensional manifold, which is the case because they have been generated using the same method. These datasets are provided with segmentation annotations for each object appearing in the scenes, which we converted to binary foreground segmentation masks in order to compute the F-measure of the predicted foreground masks.

We provide in Table 4 the average F-measure obtained on the test sets of these datasets and in Figure 4 some image samples. Considering that on these datasets the risk of overfitting is very low and the background complexity is very high, we substantially increased the number of iterations, which is set to 500 000. We do not use morphological post-processing on the ShapeStacks and ObjectsRoom datasets, because these images have a very low resolution (64×64).

Table 4. F-Measure on the Clevrtex, ShapeStacks and ObjectsRoom datasets

dataset	image size	number of	number of	average
		frames	frames	
		training set	test set on test set	F-measure
Clevrtex	128×128	40000	5000	0.78
ObjectsRoom	64×64	980000	20000	0.84
ShapeStacks	64×64	217888	46656	0.83

4.6 Computation time

We provide in Table 5 some computation time measurements, obtained using a desktop computer with an Intel Core i7 7700K@4,2GHz CPU and a Nvidia RTX 2080 TI GPU.

The training time of the autoencoder mainly depends on the size of the input images and the complexity of the background and is not proportional to the number of frames of the dataset, which makes this model attractive for long frame sequences. The model is indeed faster than PAWCS and SuBSENSE on long videos showing simple backgrounds. On short sequences with complex backgrounds, PAWCS and SuBSENSE are faster, but fail to predict accurate foreground masks (cf Table 1, PTZ category and Table 2, categories IMC, ISM, OMC, OSM).

⁴ <https://www.robots.ox.ac.uk/~vgg/data/clevrtex/>

⁵ <https://ogroth.github.io/shapestacks/>

⁶ https://github.com/deepmind/multi_object_datasets

⁷ <https://github.com/applied-ai-lab/genesis>

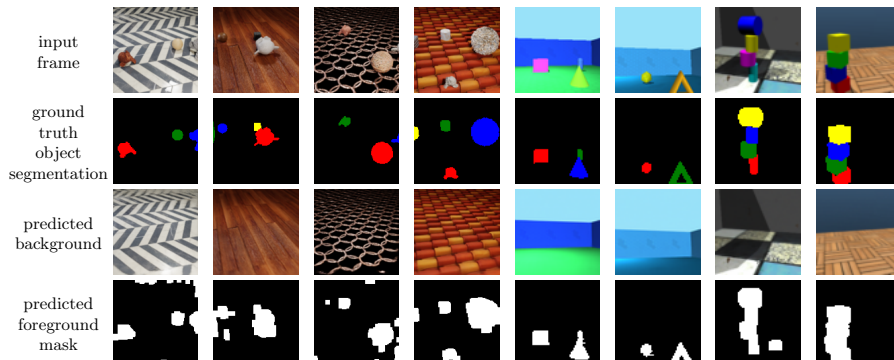


Fig. 4. Examples of background reconstruction and foreground segmentations on the datasets Clevrtex (columns 1-4), ObjectsRoom (columns 5-6) and ShapeStacks (columns 7-8)

Table 5. Computation time of the proposed model, PAWCS and SubSENSE for some sequences of the CDnet and BMC datasets

sequence name	highway	Video 009	blizzard	zoomin zoomout	continuous pan
image size	240x320	288x352	480x720	240x320	480x704
number of frames	1700	107817	7000	1130	1700
background complexity	simple	simple	simple	complex	complex
computation times (seconds)					
AE-NE (proposed model)					
- training	173	197	783	2716	14221
- backgrounds and masks generation	7	578	125	5	37
- total	180	775	908	2721	14258
SuBSENSE	98	7093	1333	68	393
PAWCS	182	13021	2418	150	1013

4.7 Ablation study

In order to assess the impact of the various model features described in this paper, we have implemented several modifications of the proposed model and measured the average F-measure (FM) of these models on the CDnet2014 dataset. The results of these experiments are provided in Table 6.

They show that the design of the loss function and the use of the background noise estimation layer have a substantial impact on the accuracy of the model. More precisely, performing background reconstruction without using the background noise estimation has a very negative impact on the categories dynamic background (FM: 0.078), turbulence (FM: 0.259), pan-tilt-zoom (FM: 0.432) and low frame-rate (FM: 0.474), but the other categories of the dataset are not significantly impacted by this modification.

The improvement associated to post-processing is also significant, as already observed for other unsupervised background subtraction methods [51].

The model remains competitive on CDnet if the background complexity of all frames sequence is set to simple, an option which may be considered if computation time is an issue and it is known that the camera is fixed.

Table 6. Evaluation of various ablations of the proposed model

model description	average F-measure on the reference CDnet dataset	evolution vs model
proposed model (reference)	0.7841	
modified models :		
- no bootstrap weights ($w_{n,i,j}^{\text{bootstrap}}$ set to 1)	0.2771	-64,6 %
- inference without using the background noise estimation (α_2 set to 0)	0.6220	-20,7 %
- $w_{n,i,j}^{\text{bootstrap}}$ set to 1 and α_2 set to 0	0.4557	-41,9%
- training with L2 reconstruction loss, α_2 set to 0	0,3384	-56,8 %
- inference without morphological post-processing	0.7170	-8.5%
- all backgrounds are considered as simple (τ_0 set to 1)	0,7397	-5,6 %

4.8 Image samples

We provide in Figure 5 some samples of background reconstruction, with the associated predicted foreground mask, and a comparison with foreground masks obtained using PAWCS and SuBSENSE. Other samples are provided in the Appendix.

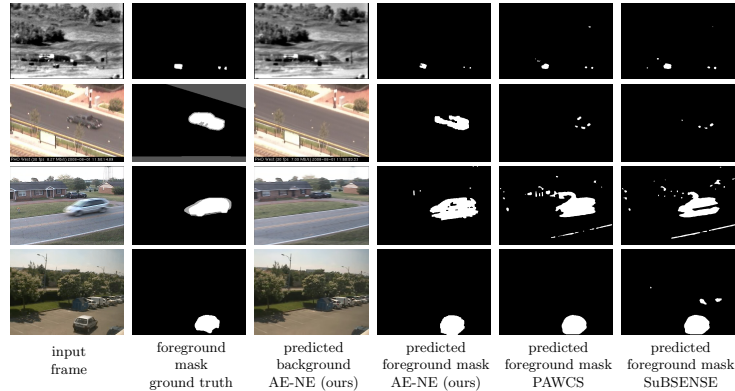


Fig. 5. Examples of background reconstruction and foreground segmentation produced using the proposed model and comparison with PAWCS and SuBSENSE

5 Conclusion

We have proposed in this paper a new fully unsupervised dynamic background reconstruction and foreground segmentation model which does not use any tem-

poral or motion information. It is on average more accurate than available unsupervised models for background subtraction, significantly improves upon the state of the art on videos taken from a moving camera and is able to perform background reconstruction on some non-video image datasets.

Future works include using the proposed model to perform unsupervised object detection on real world scenes with complex backgrounds.

References

1. Gianni Allebosch, David Van Hamme, Francis Deboeverie, Peter Veelaert, and Wilfried Philips. C-EFIC: Color and Edge Based Foreground Background Segmentation with Interior Classification. pages 433–454, 2016.
2. Olivier Barnich and Marc Van Droogenbroeck. ViBE: A powerful random technique to estimate the background in video sequences. *ICASSP, IEEE International Conference on Acoustics, Speech and Signal Processing - Proceedings*, pages 945–948, 2009.
3. Daniel Berjón, Carlos Cuevas, Francisco Morán, and Narciso García. Real-time nonparametric background subtraction with tracking-based foreground update. *Pattern Recognition*, 74:156–170, 2018.
4. Simone Bianco, Gianluigi Ciocca, and Raimondo Schettini. How far can you get by combining change detection algorithms? *Lecture Notes in Computer Science (including subseries Lecture Notes in Artificial Intelligence and Lecture Notes in Bioinformatics)*, 10484 LNCS:96–107, 2017.
5. Himani K Borse and Bharati Patil. Background Subtraction with Dirichlet process Gaussian Mixture Model (DP-GMM) for Motion Detection. 3(7):70–75, 2015.
6. Thierry Bouwmans. Traditional and recent approaches in background modeling for foreground detection: An overview. *Computer Science Review*, 11-12:31–66, 2014.
7. M Braham, S Pierard, and M Van Droogenbroeck. Semantic background subtraction. *Ieee*, pages 4552–4556, 2017.
8. Filiz Bunyak, Kannappan Palaniappan, Sumit Kumar Nath, and Gunasekaran Seetharaman. Flux tensor constrained geodesic active contours with sensor fusion for persistent object tracking. *Journal of Multimedia*, 2(4):20–33, 2007.
9. Emmanuel J. Candès, Xiaodong Li, Yi Ma, and John Wright. Robust principal component analysis? *Journal of the ACM*, 58(3), 2011.
10. Remy Chang, Tarak Gandhi, and Mohan M. Trivedi. Vision modules for a multi-sensory bridge monitoring approach. *IEEE Conference on Intelligent Transportation Systems, Proceedings, ITSC*, pages 971–976, 2004.
11. Andrew Tzer Yeu Chen, Morteza Biglari-Abhari, and Kevin I.Kai Wang. SuperBE: computationally light background estimation with superpixels. *Journal of Real-Time Image Processing*, 16(6):2319–2335, 2019.
12. Carlos Cuevas, Eva María Yáñez, and Narciso García. Labeled dataset for integral evaluation of moving object detection algorithms: LASIESTA. *Computer Vision and Image Understanding*, 152:103–117, 2016.
13. Farcas Diana and Thierry Bouwmans. Background modeling via a supervised subspace learning To cite this version : University of La Rochelle. 2010.
14. Ahmed Elgammal, David Harwood, and Larry Davis. Non-parametric model for background subtraction. *Lecture Notes in Computer Science (including subseries Lecture Notes in Artificial Intelligence and Lecture Notes in Bioinformatics)*, 1843:751–767, 2000.

15. Tarek Elguebaly and Nizar Bouguila. Finite asymmetric generalized Gaussian mixture models learning for infrared object detection. *Computer Vision and Image Understanding*, 117(12):1659–1671, 2013.
16. Martin Engelcke, Oiwi Parker Jones, and Ingmar Posner. GENESIS-V2: Inferring Unordered Object Representations without Iterative Refinement. 2021.
17. Amirreza Farnoosh, Behnaz Rezaei, and Sarah Ostadabbas. Deeppbm: Deep probabilistic background model estimation from video sequences. *arXiv*, 2019.
18. Alberto Faro, Daniela Giordano, and Concetto Spampinato. Adaptive background modeling integrated with luminosity sensors and occlusion processing for reliable vehicle detection. *IEEE Transactions on Intelligent Transportation Systems*, 12(4):1398–1412, 2011.
19. Belmar Garcia-Garcia, Thierry Bouwmans, and Alberto Jorge Rosales Silva. Background subtraction in real applications: Challenges, current models and future directions. *Computer Science Review*, 35:100204, 2020.
20. Jhony H. Giraldo and Thierry Bouwmans. GraphBGS: Background subtraction via recovery of graph signals. *Proceedings - International Conference on Pattern Recognition*, pages 6881–6888, 2020.
21. Oliver Groth, Fabian B. Fuchs, Ingmar Posner, and Andrea Vedaldi. ShapeStacks: Learning Vision-Based Physical Intuition for Generalised Object Stacking. *Lecture Notes in Computer Science (including subseries Lecture Notes in Artificial Intelligence and Lecture Notes in Bioinformatics)*, 11205 LNCS:724–739, 2018.
22. Tom S.F. Haines and Tao Xiang. Background subtraction with dirichletprocess mixture models. *IEEE Transactions on Pattern Analysis and Machine Intelligence*, 36(4):670–683, 2014.
23. Paul Henderson and Christoph H. Lampert. Unsupervised object-centric video generation and decomposition in 3D. *Advances in Neural Information Processing Systems*, 2020-Decem(Section 3), 2020.
24. Martin Hofmann, Philipp Tiefenbacher, and Gerhard Rigoll. Background segmentation with feedback: The pixel-based adaptive segmenter. *IEEE Computer Society Conference on Computer Vision and Pattern Recognition Workshops*, pages 38–43, 2012.
25. Sajid Javed, Arif Mahmood, Somaya Al-Maadeed, Thierry Bouwmans, and Soon Ki Jung. Moving Object Detection in Complex Scene Using Spatiotemporal Structured-Sparse RPCA. *IEEE Transactions on Image Processing*, 28(2):1007–1022, 2019.
26. Sajid Javed, Arif Mahmood, Thierry Bouwmans, and Soon Ki Jung. Background-Foreground Modeling Based on Spatiotemporal Sparse Subspace Clustering. *IEEE Transactions on Image Processing*, 26(12):5840–5854, 2017.
27. Jindong Jiang, Sepehr Janghorbani, Gerard de Melo, and Sungjin Ahn. SCALOR: Generative World Models with Scalable Object Representations. 2019.
28. Rishabh Kabra, Chris Burgess, Loic Matthey, Raphael Lopez Kaufman, Klaus Greff, Malcolm Reynolds, and Alexander Lerchner. Multi-Object Datasets. <https://github.com/deepmind/multi-object-datasets/>, 2019.
29. Rudrika Kalsotra and Sakshi Arora. Background subtraction for moving object detection: explorations of recent developments and challenges. *Visual Computer*, (0123456789), 2021.
30. Laurynas Karazija, Iro Laina, and Christian Rupprecht. ClevrTex: A Texture-Rich Benchmark for Unsupervised Multi-Object Segmentation. (NeurIPS), 2021.
31. Kyungnam Kim, Thanarat H. Chalidabhongse, David Harwood, and Larry Davis. Background modeling and subtraction by codebook construction. *Proceedings - International Conference on Image Processing, ICIP*, 2:3061–3064, 2004.

32. Sang Ha Lee, Gyu Cheol Lee, Jisang Yoo, and Soonchul Kwon. WisenetMD: Motion detection using dynamic background region analysis. *Symmetry*, 11(5), 2019.
33. Haifeng Li, Tao Jiang, and Keshu Zhang. Efficient and robust feature extraction by maximum margin criterion. *Advances in Neural Information Processing Systems*, 17(1):157–165, 2004.
34. Long Ang Lim and Hacer Yalim Keles. Learning multi-scale features for foreground segmentation. *Pattern Analysis and Applications*, 23(3):1369–1380, 2020.
35. Long Ang Lim and Hacer Yalim Keles. Foreground segmentation using convolutional neural networks for multiscale feature encoding. *Pattern Recognition Letters*, 112:256–262, 2018.
36. Citable Link and Darren E Butler. Real-Time Adaptive Foreground / Background Segmentation. 2005(14), 2018.
37. Xin Liu, Guoying Zhao, Jiawen Yao, and Chun Qi. Background subtraction based on low-rank and structured sparse decomposition. *IEEE Transactions on Image Processing*, 24(8):2502–2514, 2015.
38. Lucia Maddalena and Alfredo Petrosino. A self-organizing approach to background subtraction for visual surveillance applications. *IEEE Transactions on Image Processing*, 17(7):1168–1177, 2008.
39. Lucia Maddalena and Alfredo Petrosino. The SOBS algorithm: What are the limits? *IEEE Computer Society Conference on Computer Vision and Pattern Recognition Workshops*, pages 21–26, 2012.
40. Julien Mairal, Rodolphe Jenatton, Guillaume Obozinski, and Francis Bach. Network flow algorithms for structured sparsity. *Advances in Neural Information Processing Systems 23: 24th Annual Conference on Neural Information Processing Systems 2010, NIPS 2010*, pages 1–9, 2010.
41. Murari Mandal and Santosh Kumar Vipparthi. Scene Independency Matters: An Empirical Study of Scene Dependent and Scene Independent Evaluation for CNN-Based Change Detection. *IEEE Transactions on Intelligent Transportation Systems*, pages 1–14, 2020.
42. Murari Mandal and Santosh Kumar Vipparthi. An Empirical Review of Deep Learning Frameworks for Change Detection: Model Design, Experimental Frameworks, Challenges and Research Needs. *IEEE Transactions on Intelligent Transportation Systems*, pages 1–22, 2021.
43. V. Mondéjar-Guerra, J. Rouco, J. Novo, and M. Ortega. An end-to-end deep learning approach for simultaneous background modeling and subtraction. *30th British Machine Vision Conference 2019, BMVC 2019*, pages 1–12, 2020.
44. Dibyendu Mukherjee and Q. M. Jonathan Wu. Real-time video segmentation using student’s t mixture model. *Procedia Computer Science*, 10:153–160, 2012.
45. Nuria M Oliver, Barbara Rosario, Alex P Pentland, and Senior Member. A Bayesian Computer Vision System for Modeling Human Interactions. 22(8):831–843, 2000.
46. Montse Pardàs and Gemma Canet. Refinement network for unsupervised on the scene foreground segmentation. *European Signal Processing Conference, 2021-Janua:705–709*, 2021.
47. Gani Rahmon, Filiz Bunyak, Guna Seetharaman, and Kannappan Palaniappan. Motion U-Net: Multi-cue encoder-decoder network for motion segmentation. *Proceedings - International Conference on Pattern Recognition*, pages 8125–8132, 2020.
48. Behnaz Rezaei, Amirreza Farnoosh, and Sarah Ostadabbas. G-LBM: Generative Low-Dimensional Background Model Estimation from Video Sequences. *Lecture Notes in Computer Science (including subseries Lecture Notes in Artificial Intelligence and Lecture Notes in Bioinformatics)*, 12357 LNCS:293–310, 2020.

49. Christof Ridder, Olaf Munkelt, and Harald Kirchner. Adaptive Background Estimation and Foreground Detection using Kalman Filtering. *Proceedings of the International Conference on Recent Advances in Mechatronics (ICRAM 1995)*, pages 193–199, 1995.
50. Bruno Sauvalle and Arnaud de La Fortelle. Fast and Accurate Background Reconstruction Using Background Bootstrapping. *Journal of Imaging*, 8(1), 2022.
51. Ajmal Shahbaz, Joko Hariyono, and Kang Hyun Jo. Evaluation of background subtraction algorithms for video surveillance. *2015 Frontiers of Computer Vision, FCV 2015*, 2015.
52. Arnold W M Smeulders. Efficient projection pursuit density estimation for background subtraction 3 . Projection pursuit density estimation. 0(3).
53. Andrews Sobral. BGSLibrary: An OpenCV C++ Background Subtraction Library. *IX Workshop de Visao Computacional (WVC'2013)*, (JUNE 2013):1–3, 2013.
54. Pierre Luc St-Charles, Guillaume Alexandre Bilodeau, and Robert Bergevin. SuB-SENSE: A universal change detection method with local adaptive sensitivity. *IEEE Transactions on Image Processing*, 24(1):359–373, 2015.
55. Pierre Luc St-Charles, Guillaume Alexandre Bilodeau, and Robert Bergevin. Universal Background Subtraction Using Word Consensus Models. *IEEE Transactions on Image Processing*, 25(10):4768–4781, 2016.
56. Chris Stauffer and W. E.L. Grimson. Adaptive background mixture models for real-time tracking. *Proceedings of the IEEE Computer Society Conference on Computer Vision and Pattern Recognition*, 2:246–252, 1999.
57. Maryam Sultana, Arif Mahmood, Sajid Javed, and Soon Ki Jung. Unsupervised deep context prediction for background estimation and foreground segmentation. *Machine Vision and Applications*, 30(3):375–395, 2019.
58. M. Ozan Tezcan, Prakash Ishwar, and Janusz Konrad. BSUV-Net 2.0: Spatio-Temporal Data Augmentations for Video-Agnostic Supervised Background Subtraction. *IEEE Access*, 9:53849–53860, 2021.
59. Kentaro Toyama, John Krumm, Barry Brumitt, and Brian Meyers. Wallflower: Principles and practice of background maintenance. *Proceedings of the IEEE International Conference on Computer Vision*, 1:255–261, 1999.
60. Antoine Vacavant, Thierry Chateau, Alexis Wilhelm, and Laurent Lequière. A benchmark dataset for outdoor foreground/background extraction. *Lecture Notes in Computer Science (including subseries Lecture Notes in Artificial Intelligence and Lecture Notes in Bioinformatics)*, 7728 LNCS(PART 1):291–300, 2013.
61. Rui Wang, Filiz Bunyak, Guna Seetharaman, and Kannappan Palaniappan. Static and moving object detection using flux tensor with split gaussian models - Wang et al. - 2014 - IEEE Computer Society Conference.pdf. *IEEE Change Detection Workshop, CVPR*, pages 414–418, 2014.
62. Yi Wang, Pierre Marc Jodoin, Fatih Porikli, Janusz Konrad, Yannick Benezeth, and Prakash Ishwar. CDnet 2014: An expanded change detection benchmark dataset. *IEEE Computer Society Conference on Computer Vision and Pattern Recognition Workshops*, pages 393–400, 2014.
63. Christopher Richard Wren, Ali Azarbayejani, Trevor Darrell, and Alex Paul Pentland. Pfnder: Real-Time Tracking of the Human Body. *IEEE Trans. Pattern Anal. Mach. Intell.*, 19(7):780–785, 1997.
64. John Wright, Yigang Peng, Yi Ma, Arvind Ganesh, and Shankar Rao. Robust principal component analysis: Exact recovery of corrupted low-rank matrices by convex optimization. *Advances in Neural Information Processing Systems 22 - Proceedings of the 2009 Conference*, pages 2080–2088, 2009.

65. Yizhe Wu, Oiwi Parker Jones, Martin Engelcke, and Ingmar Posner. APEX: Un-supervised, Object-Centric Scene Segmentation and Tracking for Robot Manipulation. 2021.
66. Bo Xin, Yuan Tian, Yizhou Wang, and Wen Gao. Background Subtraction via generalized fused lasso foreground modeling. *Proceedings of the IEEE Computer Society Conference on Computer Vision and Pattern Recognition*, 07-12-June:4676–4684, 2015.
67. Dongdong Zeng, Xiang Chen, Ming Zhu, Michael Goesele, and Arjan Kuijper. Background Subtraction with Real-Time Semantic Segmentation. *IEEE Access*, 7:153869–153884, 2019.
68. Shengping Zhang, Hongxun Yao, Shaohui Liu, Shengping Zhang, Hongxun Yao, Shaohui Liu, Dynamic Background, Subtraction Based, Shengping Zhang, Hongxun Yao, and Shaohui Liu. Dynamic Background Subtraction Based on Local Dependency Histogram To cite this version. 2008.
69. Wenbo Zheng, Kunfeng Wang, and Fei Yue Wang. A novel background subtraction algorithm based on parallel vision and Bayesian GANs. *Neurocomputing*, 394:178–200, 2020.

6 Appendix

6.1 Autoencoder architecture

The autoencoder is deterministic and takes as input a RGB image of size $h \times w$, and produces a RGB image (3 channels) and an error estimation map of the same size (1 channel).

The encoder and decoder structures in the proposed model are computed dynamically using as input the size (height h and width w) of the input frames of the dataset. The number of latent variables produced by the encoder is fixed to 16.

We use a fully convolutional autoencoder architecture, which appears to be more robust to overfitting than architectures including fully connected layers or locally connected layers. We add two fixed positional encoding channels as inputs to all layers of the encoder and the decoder, one channel coding for the horizontal coordinates, the other one for the vertical coordinates .

The encoder is a sequence of blocks composed of a convolution layer with kernel size 5, stride 3 and padding equal to 2, followed by a group normalization layer and a CELU nonlinearity layer. The generator is a symmetric sequence of blocks composed of transpose convolution layers with kernel size 5 and stride 3 and padding equal to 2 followed by group normalization and a CELU nonlinearity, except for the last layer where the transpose convolution layer is followed by a sigmoid to generate the final image. The number of layers of the encoder and the decoder is then equal to 5 or 6 depending on the image size (assuming that the maximum of the image height and image width is in the range 200 – 1000). The number of channels per convolutional layer is fixed according to Table 7, depending on the image size and the background complexity.

These channel distributions are motivated by the fact that a larger number of parameters is required in the generator in order to handle complex backgrounds,

Table 7. Number of channels for each layer of the encoder and decoder (excluding positional encoding input channels)

background complexity	image size max(h,w)	Encoder	Decoder
simple	200-405	(3,64,160,160,32,16)	(16,32,256,256,144,4)
simple	406-1000	(3,64,160,160,160,32,16)	(16,32,256,512,256,144,4)
complex	200-405	(3,64,160,160,16,16)	(16,16,640,640,144,4)
complex	406-1000	(3,64,160,160,160,16,16)	(16,16,640,1280,640,144,4)

but that we have experimentally observed that a large number of channels in the last layer of the encoder and the first layer of the decoder increases the risk of overfitting on foreground objects, so that reducing this number for long training schedule is necessary to improve the robustness of the auto-encoder with respect to the risk of overfitting. For example, we have measured that increasing the numbers of channels in the last hidden layer of the encoder and first hidden layer of the decoder to 160 and 256 leads to de 2,3 % degradation of the average F-Measure on the CDnet dataset.

For non-video dataset experiments, which handle small images, we use a smaller stride, set to 2 instead of 3. The autoencoder architectures for 64×64 images (ShapeStacks and ObjectRooms datasets) and 128×128 images (Clevrtex dataset) are described in Table 8 and 9:

Table 8. autoencoder architecture for 64×64 images

Encoder					Decoder				
Layer	Size	Ch	Stride	Norm./Act.	Layer	Size	Ch	Stride	Norm./Act.
Input	64	3			Input	1	16		
Conv 5 × 5	32	64	2	GroupNorm/CELU	Conv Transp 2 × 2	2	16	1	GroupNorm/CELU
Conv 5 × 5	16	160	2	GroupNorm/CELU	Conv Transp 4 × 4	4	640	2	GroupNorm/CELU
Conv 5 × 5	8	320	2	GroupNorm/CELU	Conv Transp 5 × 5	8	1280	2	GroupNorm/CELU
Conv 5 × 5	4	160	2	GroupNorm/CELU	Conv Transp 5 × 5	16	640	2	GroupNorm/CELU
Conv 4 × 4	2	16	2	GroupNorm/CELU	Conv Transp 5 × 5	32	144	2	GroupNorm/CELU
Conv 2 × 2	1	16	1	GroupNorm/CELU	Conv Transp 5 × 5	64	4	2	
					Sigmoid	64	4		

Table 9. autoencoder architecture for 128×128 images

Encoder					Decoder				
Layer	Size	Ch	Stride	Norm./Act.	Layer	Size	Ch	Stride	Norm./Act.
Input	128	3			Input	1	16		
Conv 5 × 5	64	64	2	GroupNorm/CELU	Conv Transp 2 × 2	2	16	1	GroupNorm/CELU
Conv 5 × 5	32	320	2	GroupNorm/CELU	Conv Transp 4 × 4	4	320	2	GroupNorm/CELU
Conv 5 × 5	16	640	2	GroupNorm/CELU	Conv Transp 5 × 5	8	640	2	GroupNorm/CELU
Conv 5 × 5	8	640	2	GroupNorm/CELU	Conv Transp 5 × 5	16	1280	2	GroupNorm/CELU
Conv 5 × 5	4	320	2	GroupNorm/CELU	Conv Transp 5 × 5	32	640	2	GroupNorm/CELU
Conv 4 × 4	2	16	2	GroupNorm/CELU	Conv Transp 5 × 5	64	144	2	GroupNorm/CELU
Conv 2 × 2	1	16	1	GroupNorm/CELU	Conv Transp 5 × 5	128	4	2	
					Sigmoid	128	4		

6.2 Implementation details

The proposed model is implemented using Python and the Pytorch framework. The associated code will be made available on the Github platform. Optimization is performed using the Adam optimizer with a learning rate of $5 \cdot 10^{-4}$ and batch size equal to 32. The learning rate is divided by 10 when the number of optimization iterations reaches 80% of the total number of iterations. The same set of hyperparameters is used for the experiments on CDnet, LASIESTA and BMC datasets, i.e. $\beta = 6$, $r = 75$, $\tau_0 = 0.24$, $\tau_1 = 0.25$, $\alpha_1 = 96/255$, $\alpha_2 = 7$, $N_{\text{eval}} = 2000$, $B_{\text{eval}} = 480$, $N_{\text{simple}} = 2500$, $N_{\text{complex}} = 24000$, $E_{\text{complex}} = 20$. These hyperparameter values as well as the channel distributions described in Table 7 were found empirically to give good results, although a full hyperparameter and architecture search has not been performed and is beyond the scope of this paper.

For non-video dataset experiments, which take small images (64×64 and 128×128) as inputs, the batch size and learning rate are increased to 128 and $2 \cdot 10^{-3}$, the number of iterations N_{complex} is set to 500 000 and no morphological post-processing is performed on 64×64 images. The other hyperparameters remain the same.

6.3 Additional image samples

We provide in figures 6 – 12 additional samples of background reconstruction and foreground segmentation obtained using the proposed model.

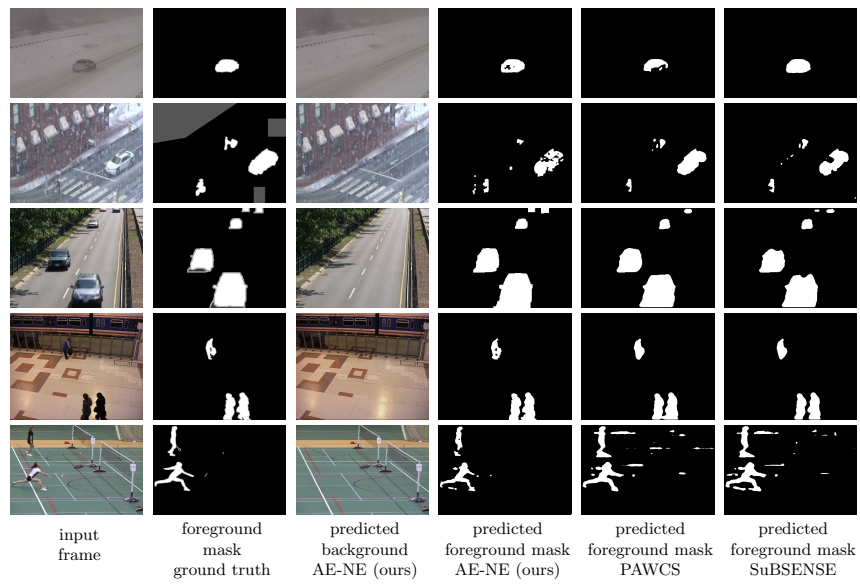


Fig. 6. Examples of background reconstruction and foreground segmentation on the CDnet 2014 dataset produced using the proposed model and comparison with PAWCS and SuBSENSE

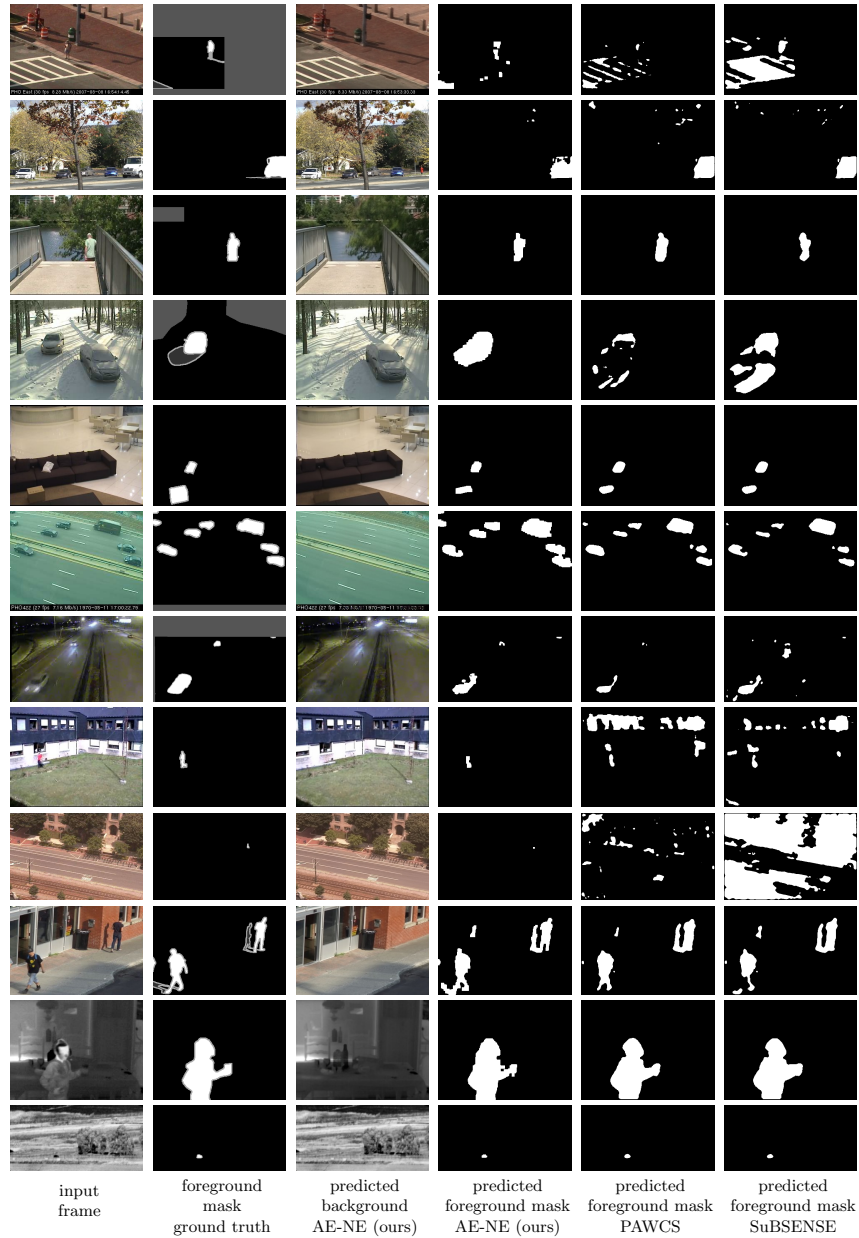


Fig. 7. Examples of background reconstruction and foreground segmentation on the CDnet 2014 dataset produced using the proposed model and comparison with PAWCS and SuBSENSE

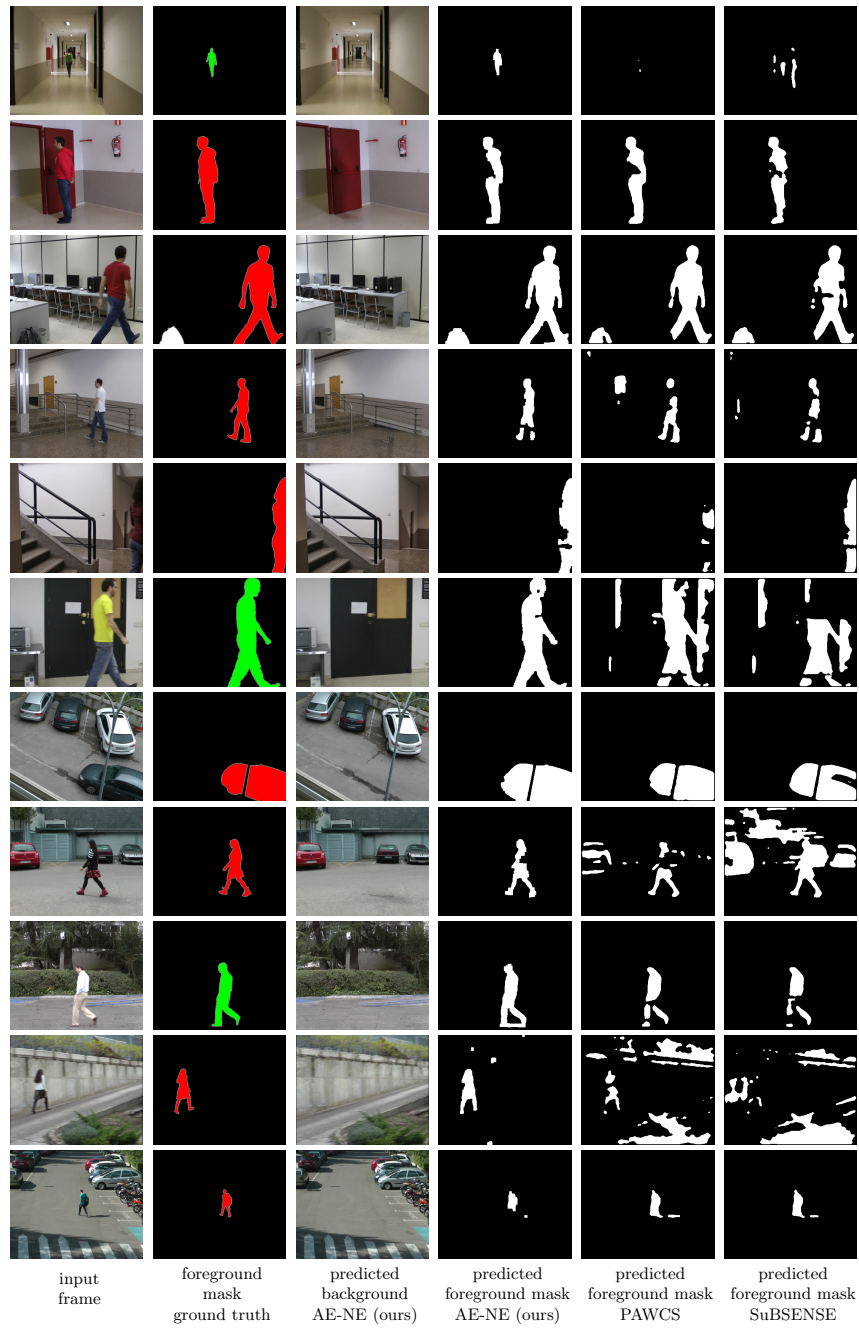


Fig. 8. Examples of background reconstruction and foreground segmentation on the LASIESTA dataset produced using the proposed model and comparison with PAWCS and SuBSENSE

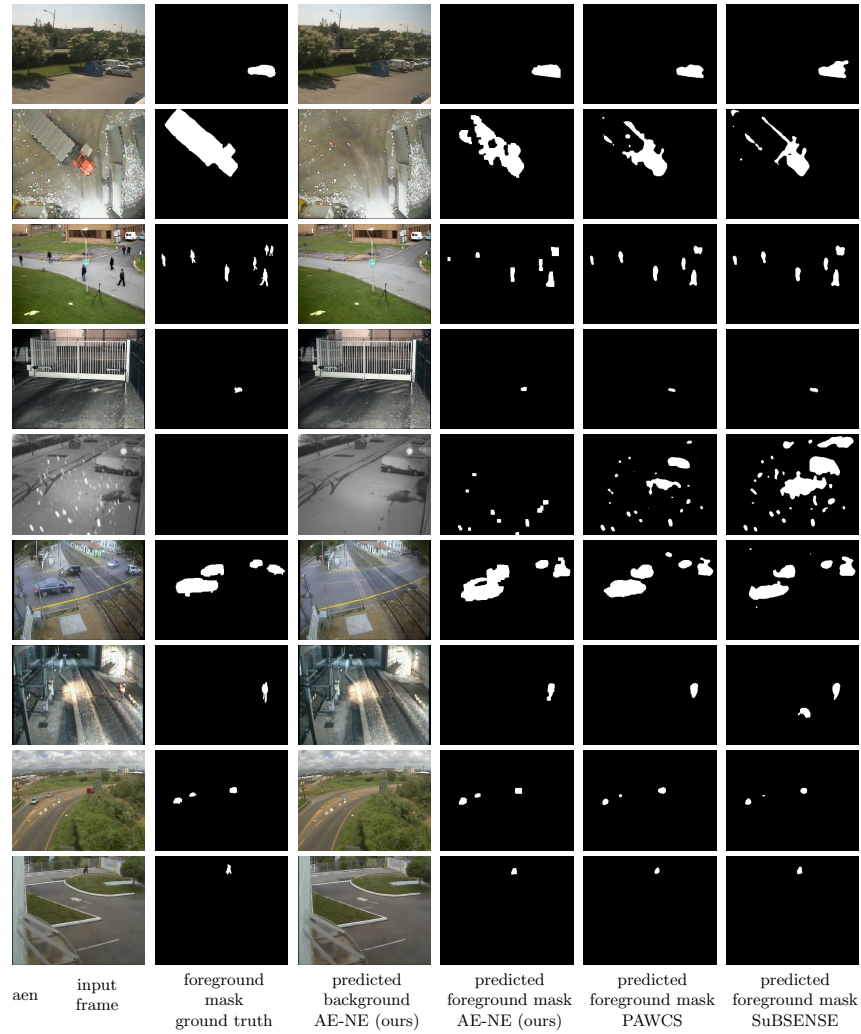


Fig. 9. Examples of background reconstruction and foreground segmentation on the BMC 2012 dataset produced using the proposed model and comparison with PAWCS and SuBSENSE

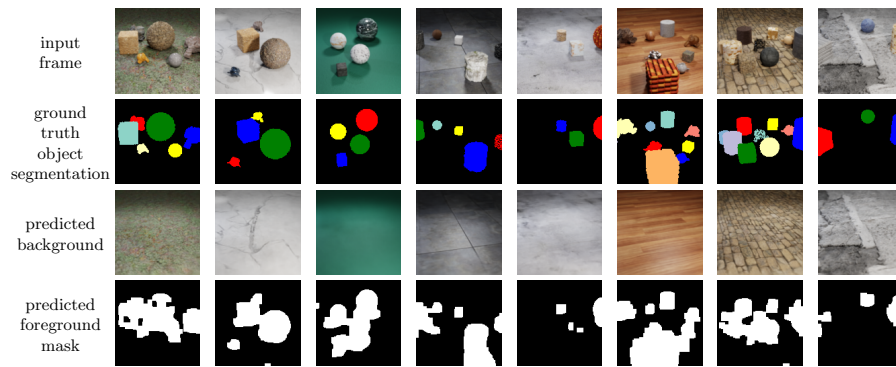


Fig. 10. Examples of background reconstruction and foreground segmentation on ClevrTex dataset

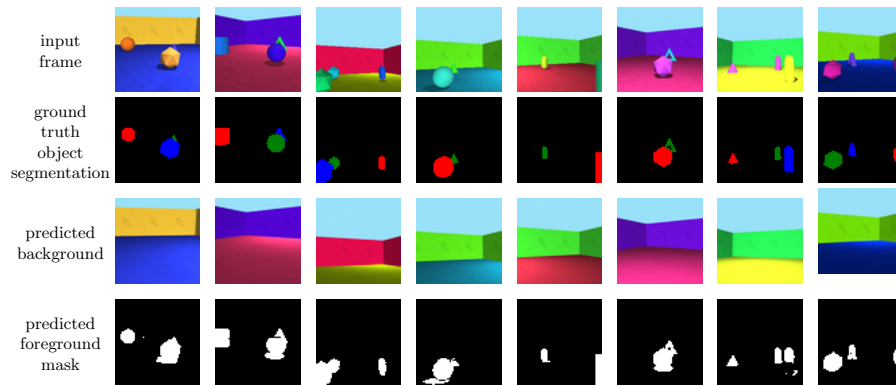


Fig. 11. Examples of background reconstruction and foreground segmentation on ObjectsRoom dataset

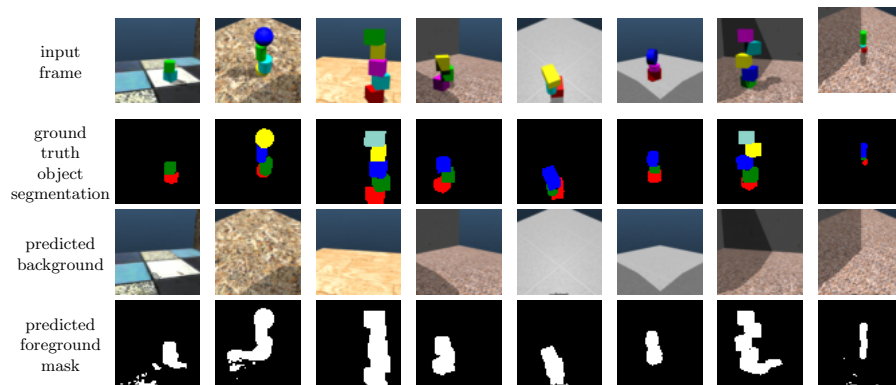


Fig. 12. Examples of background reconstruction and foreground segmentation on ShapeStacks dataset